Adaptive Unit Protection for Lines Connecting Large Solar Plants using Incremental Current Ratio

Arghadeep Chowdhury*, Subhadeep Paladhi* and Ashok Kumar Pradhan, *Senior Member, IEEE*

***Abstract*—Control schemes in a solar plant complying with different grid codes modulate the output voltage and current significantly during fault. In this paper, the issue with conventional current differential approaches for the line connecting large solar plant is analyzed and a new protection technique using both end incremental current phasors is proposed. The proposed method uses two criteria to identify the internal faults in such connectivity. The first criterion is based on the ratio of both end incremental phase current phasors and the second one uses the magnitude ratio of positive sequence incremental currents. Both the criteria are adaptive to line terminal currents and complement each other enriching the method applicable for any system condition. Performance of the proposed method is tested for different internal and external fault cases and found to be accurate. The compatibility of the proposed method is also validated using real-time simulator. Comparative assessment with conventional current differential techniques reveals the superiority of the proposed approach.**

***Index Terms*—Line differential protection, power system faults, adaptive relaying, solar photovoltaic power plant.**

I. Introduction

PRESENT environmental concern compels renewable energy integration in large scale to high voltage transmission network using interfacing converter and transformer [1], [2]. In order to maintain the reliability of power systems with renewable sources like solar plants, different control schemes are being applied to the converters. To satisfy the requirement as imposed by grid codes, large-scale solar plants are set to ride through the low voltage situation even during fault [3]. Such converter interfaced sources in the network modulate the voltage and current signals significantly during fault. Such a change in the fault behavior of a power system impels the available protection schemes to be under scrutiny.

Impacts of converter interfaced renewable plants (CIRP) on the performance of directional overcurrent, distance, current differential and faulted phase selection schemes are analyzed in [4]–[8]. The availability of fibre-optic and digital microwave communication channels prefers current differential schemes to be widely used for transmission lines for high speed decision for 100% of the line, high sensitivity and reliable protection [9], [10]. Such a scheme is not affected by power swing, load encroachment, and CVT transient [8]. The current differential principle assumes homogeneity of the system, which may not be true always in the presence of renewable sources connected to any end of the line. Converter control operation associated with renewable plants may result in significant phase angle difference between both end currents, even for internal faults. Limited performance of conventional current differential relay for line-to-line faults due to fault current angle modulation by CIRP is demonstrated in [11], [12]. Due to fault current limitation by the CIRP interfacing converters, the sensitivity of current differential relay is also affected. A negative sequence component-based current differential technique is proposed for discrimination of internal and external faults [13]. Such a technique finds limitations in the case of balanced faults and in the presence of renewable plants embedded with dual current control schemes. A technique based on similarity of currents at both sides of the protected line is proposed to identify faults correctly in a CIRP connected line [12]. The technique uses a high value of threshold to eliminate transient capacitive currents resulting in a reduction in the sensitivity. Based on the fault current limiting feature of CIRP interfacing converters, a current amplitude-based protection solution is provided in [14], which finds limitations in case of high resistance ground faults. The performances of the above techniques are found to be accurate in specific fault situations and difficult to generalize, especially for changes in system conditions and control schemes associated with the converters interfacing different types of CIRPs. Furthermore, the techniques are tested only for the fault cases, where grid side contribution dominates significantly. Large-scale CIRP integration resulting in CIRP side fault current to be comparable to the grid side current may also lead the current differential relay to malfunction at times. Such an issue is not addressed by any of the techniques mentioned above. Therefore a new method is sought for proper protection of lines connecting large-scale CIRPs, like solar plants or so.

In this work, the issue associated with conventional current differential relaying is analyzed for fault conditions, when the grid side current becomes comparable to the current contributed by the large solar plant connected to the line. A protection technique is proposed for the correct identification of internal faults in the line with such connectivity using two criteria. The first criterion is based on the ratio of incremental phase currents at the two ends. The magnitude ratio of the positive sequence incremental currents is used in the second criterion. The restraining zone is adapted to the change in grid side terminal current in criterion-1 and solar plant side current in criterion-2. Such adaptivity in the protection scheme provides high sensitivity for different system conditions, without compromising security. Both the criteria complementing each other make the method applicable to lines connecting any renewable or conventional sources and irrespective of the associated control schemes. Performance of the proposed method is tested on solar plant integrated modified 39-bus New England system using PSCAD/EMTDC simulation data for

The work is supported in part by DST, India, under Grant DST/RCU/JVCCE/2015/02(C).

**A. Chowdhury and S. Paladhi are co-first authors with equal contribution*. The authors are with the Department of Electrical Engineering, Indian Institute of Technology, Kharagpur 721302, India (e-mail: argha8900397358.2012@gmail.com, paladhisubha91@gmail.com, akpradhan@ee.iitkgp.ac.in).

different internal and external faults and found to be accurate. The method is also tested for two more standard systems with different renewable sources with change in grid code compliance. The method maintains security during external faults with current transformer (CT) saturation. Performance of the proposed method is validated using OPAL-RT real-time simulator. The comparative assessment reveals the superiority of the proposed method.

II. Problem Statement

A two bus equivalent transmission network integrating a solar plant to the grid is shown in Fig. 1(a). The plant consists of multiple photovoltaic (PV) units, each connected to the collector bus through a DC/AC inverter and a step-up transformer as shown in the figure.

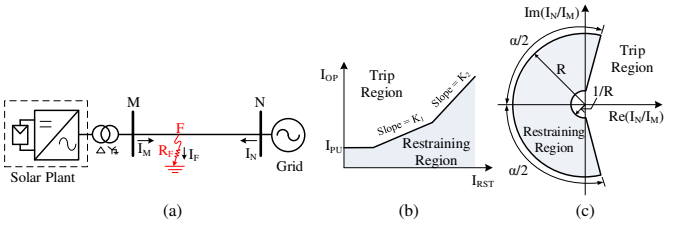

Fig. 1. (a)Transmission line connecting solar plant and protected by current differential relay with (b) percentage bias and (c) α-plane characteristics.

Line MN in the system is protected by a current differential scheme using current phasors of both ends (I_M and I_N). Relay using such a protection principle generates a trip signal for the line end circuit breakers using percentage bias characteristic as in Fig. 1(b) with operating current ($I_{OP} = |I_M + I_N|$), restraining current ($I_{RST} = |I_M - I_N|$), slopes of the line (K_1 and K_2) and pickup current (I_{PU}) [15]. Line differential relays also use the current ratio ($\frac{I_N}{I_M}$) with α-plane characteristic, as shown in Fig. 1(c). This provides a high tolerance level to channel asymmetry, line-charging current and CT saturation without sacrificing sensitivity for internal faults [15]. In this work, performances of both relaying approaches are evaluated for the line in Fig. 1(a).

The inverter interfacing the solar plant is controlled in synchronous reference frame, as shown in Fig. 2 [16], [17]. The grid side and converter side voltages are denoted by V_{GRID} and V_{INV} respectively. In order to decouple the solar plant from the grid-side, feedforward compensation is applied to the output of PI controllers, as shown in Fig. 2 by the blue arrows. This maintains the voltage across the filter to be balanced even during unbalanced situations on the grid side and consequently generates balanced currents in output. The control parameters with filter details are provided in the Appendix. The solar plant is modeled satisfying North American grid codes (NA-GCs) and set to ride through fault maintaining the power factor range from 0.95 leading to 0.95 lagging [18]. The proposed method is also tested for the plant complied with European Union Grid Code (EU-GC), which imposes priority on reactive power support in low voltage situations like faults. As an example of EU-GC, the low voltage ride through (LVRT) curve followed by German grid code is shown in Fig. 3(a) [19]. The reactive current requirement for such a situation is shown in Fig. 3(b). V_n and I_n in the figure are the nominal voltage and current

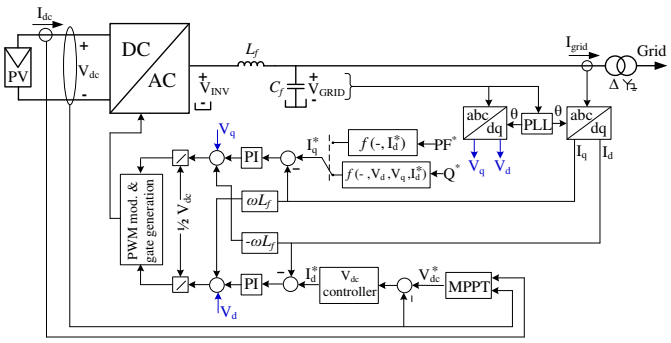

Fig. 2. Control scheme applied to the solar plant.

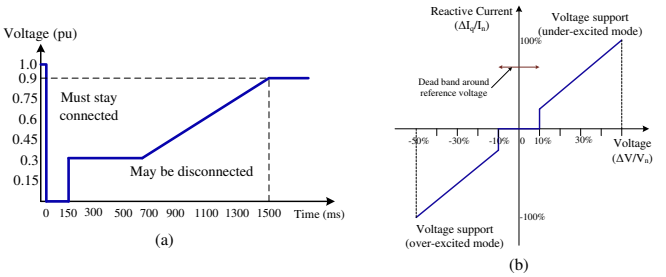

Fig. 3. (a) LVRT curve and (b) reactive current requirement of the German GC for solar plants during faults.

respectively. ΔI_q and ΔV are the changes in the reactive current and voltage during faults.

The equivalent model of the system of Fig. 1(a) is represented in Fig. 4 during prefault condition. The line impedance is presented by Z_{1L}. The positive sequence model of the grid is represented using a voltage source (E_{1G}) with an internal impedance (Z_{1G}) connected in series. The grid-feeding power converter connecting solar plant is represented with a dependent current source (I_{1S}^{pre}) in parallel with a high impedance (Z_{1PV}), as shown in the network diagram [6], [20]. Subscript '1' represents the positive sequence component.

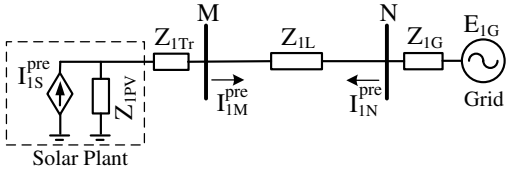

Fig. 4. Equivalent model of solar plant integrated transmission network.

In the next section, the performance of current differential relay is analyzed for different internal fault situations.

A. Differential relaying for severe internal faults

Current differential relays operate for individual phase current, which is a combination of three sequence components during an unbalanced fault. Solar plant being connected to the grid through dYg type transformer, the zero sequence current becomes independent of solar plant status and control scheme. Thus the impact of solar plant control becomes minimum when the zero sequence current dominates over the other sequence currents, which is common for ground faults with such converter based weak sources. In order to evaluate

the effect of solar plant control on current differential relay performance, an ungrounded phase-to-phase fault (BC type) is created in line MN of the system in Fig.1(a).

Fig.5 shows the sequence network of the system in Fig.1(a) for a BC fault created in line MN at a distance of x pu from bus M. Z_{2eq} is the equivalent negative sequence impedance of the network and is connected in series with fault resistance (R_F). Superscript 'f' indicates the measurement during fault.

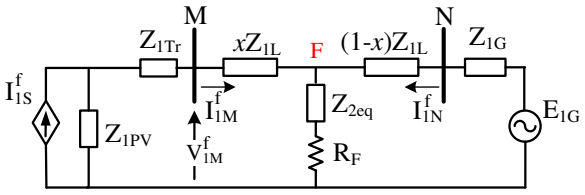

Fig. 5. Sequence network of solar plant integrated network for BC fault.

High value of Z_{1PV} results in $I^f_{1M} \approx I^f_{1S}$. With balanced current controller for solar plant, Z_{2eq} becomes equal to $((1-x)Z_{2L} + Z_{2G})$. Considering these for a BC fault with $R_F \approx 0$, current at bus N can be expressed as,

$$I^f_{1N} = \frac{E_{1G}}{2\left(Z_{1G} + (1-x)Z_{1L}\right)} - \frac{I^f_{1S}}{2} \tag{1}$$

For such a situation, V^f_{1M} in Fig. 5 can be expressed as,

$$V^f_{1M} = xZ_{1L}I^f_{1M} + Z_{2eq}(I^f_{1M} + I^f_{1N}). \tag{2}$$

substituting I^f_{1M}, I^f_{1N} and Z_{2eq} in (2) and considering grid to be strong (i.e. $|Z_{1G}| << |Z_{1L}|$), V^f_{1M} can be rewritten as,

$$V^f_{1M} = (1+x)\frac{Z_{1L}}{2}I^f_{1S} + \frac{E_{1G}}{2}. \tag{3}$$

Comparing real and imaginary parts in (3) and considering transmission impedance angle close to $\frac{\pi}{2}$, the phase angle of V^f_{1M}, denoted by θ^f_{1M}, can be expressed as,

$$\theta^f_{1M} = sin^{-1}\frac{(1+x)|I^f_{1S}||X_{1L}|cos(\phi_f)}{|E_{1G}|}. \tag{4}$$

where ϕ_f is the angle of I^f_{1M} with respect to V^f_{1M}.

With balanced solar plant controller during BC fault, phase currents at bus M contain only positive sequence component. Thus I^f_{BM} and I^f_{CM} during fault can be expressed as in (5).

$$\begin{aligned} I^f_{BM} &= |I^f_{1M}|\angle(\theta^f_{1M} - \phi_f - (2\pi/3)) \\ I^f_{CM} &= |I^f_{1M}|\angle(\theta^f_{1M} - \phi_f + (2\pi/3)) \end{aligned} \tag{5}$$

Applying Kirchoff's voltage law in the faulted loop from grid side, phase-B and phase-C current at bus N are expressed as,

$$I^f_{BN} = -I^f_{CN} = \frac{E_{BG} - E_{CG}}{2[(1-x)Z_{1L} + Z_{1G}]}. \tag{6}$$

where E_{BG} and E_{CG} are the phase-B and phase-C internal voltages of the grid. $2[(1-x)Z_{1L} + Z_{1G}]$ is the impedance of the faulted loop. The internal voltages of a strong grid remain almost constant and balanced even during fault. Thus I^f_{BN} and I^f_{CN} of (6) can be rewritten as,

$$I^f_{BN} = |I^f_N|\angle -\left(\frac{\pi}{2} + \theta_Z\right) \quad \text{and} \quad I^f_{CN} = |I^f_N|\angle\left(\frac{\pi}{2} - \theta_Z\right) \tag{7}$$

where $I^f_N = \frac{\sqrt{3}E_{1G}}{2[(1-x)Z_{1L}+Z_{1G}]}$ and θ_Z is the phase angle of $2[(1-x)Z_{1L} + Z_{1G}]$.

With the I^f_{CM} and I^f_{CN} values obtained from (5) and (7) respectively, the operating and restraining currents in phase-C can be expressed as,

$$\begin{aligned} I_{OP} &= \sqrt{|I^f_{1M}|^2 + |I^f_N|^2 + 2|I^f_{1M}||I^f_N|cos\theta_C} \\ I_{RST} &= \sqrt{|I^f_{1M}|^2 + |I^f_N|^2 - 2|I^f_{1M}||I^f_N|cos\theta_C} \end{aligned} \tag{8}$$

where $\theta_C = (\theta^f_{1M} - \phi_f + \theta_Z + (\pi/6))$, is the angle between I^f_{CM} and I^f_{CN}. For a current differential relay having a bias setting K (as in Fig. 1(b)) and $I_{OP} > I_{PU}$, the trip condition in phase-C (i.e. $I_{OP} \geq KI_{RST}$) can be expressed as,

$$4|I^f_{1M}||I^f_N|cos(\theta_C) \geq (K^2-1)[|I^f_{1M}|^2 + |I^f_N|^2] \tag{9}$$

Considering $\theta_Z \approx (\pi/2)$ for a high voltage transmission network, (9) can be simplified as,

$$sin(\theta^f_{1M} - \phi_f + \frac{\pi}{6}) < (1-K^2)[\frac{1+|D|^2}{4|D|}] \tag{10}$$

where $|D|$ is given by

$$|D| = \frac{|I^f_N|}{|I^f_{1M}|} \approx \frac{\sqrt{3}|E_{1G}|}{|I^f_{1S}||2[(1-x)Z_{1L} + Z_{1G}]|} \tag{11}$$

For a strong grid, $|E_{1G}|$ remains constant with a low value of Z_{1G}. Thus θ^f_{1M} in (4) and $|D|$ in (11) depends on Z_{1L}, $|I^f_{1S}|$ and x. As Z_{1L} depends on the line length and $|I^f_{1S}|$ varies with the plant capacity (associated with number of operating units, solar irradiance etc.), the operating condition of differential relay in (10) becomes a function of these parameters and the relations can be described as follows.

- *Variation in line length (L)*: Z_{1L} being proportional to the line length, θ^f_{1M} in (4) increases with it, whereas $|D|$ in (11) decreases for the same. Thus relay with the tripping condition in (10) becomes prone to maloperation for long lines connecting such a plant.
- *Variation in plant capacity (P)*: The solar plant output current is the summation of the individual units in the plant. So $|I^f_{1S}|$ is directly proportional to the number of available operating units or plant generation. Thus the effect of plant capacity is similar to line length and the chance of relay maloperation increases with higher plant capacity.
- *Variation in fault location (x)*: It is evident from (4) and (11) that both θ^f_{1M} and $|D|$ increase with x. But increment in right hand side of (10) is more than left hand side with increase in x. Therefore, the chances of relay maloperation decreases with high value of x.

These are demonstrated in Fig.6 for BC faults created on line MN of Fig. 1(a). The ratio of I_{OP}/I_{Th} is provided in Fig. 6 (a), where $I_{Th} = KI_{RST} + I_{PU}$ with $K = 0.4$ [21]. $I_{OP} < I_{Th}$ in percentage biased differential relay and current ratio inside α-plane characteristic [22] individually indicates maloperation for the approaches respectively. Results also show that α-plane based differential relay is more prone to maloperation with such a connectivity due to high tolerance level. Line length of 200 km and plant capacity of 400 MW is considered for per unit conversion in Fig. 6 (a). Each symbol associated with a parameter represents same 'pu' value for both the cases, which can be obtained from Fig. 6 (a).

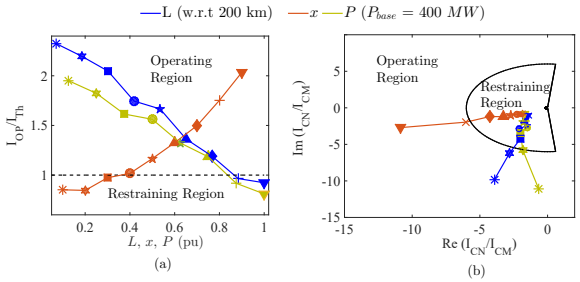

Fig. 6. Performance of (a) percentage biased and (b) α-plane based differential relay with variations in L, x, and P.

B. For internal faults with high fault resistance

Impact of a high resistance fault [23] in the line connecting solar plant is analyzed in this section for a phase-A-to-ground (AG) fault in line MN of Fig. 1(a). Equivalent sequence network for the AG fault is shown in Fig. 7. Z_{0eq} is the equivalent zero sequence impedance of the network. Considering the current through Z_{1PV} to be negligible, the positive sequence fault currents at both ends of the line MN are expressed as

$$I^f_{1M}=I^f_{1S} \text{ and } I^f_{1N}=\frac{E_{1G}}{(1-x)Z_{1L}+Z_{2eq}+Z_{0eq}+3R_F+Z_{1G}}-kI^f_{1S} \quad (12)$$

where, the distribution factor (k) is represented as

$$k=\frac{Z_{2eq}+Z_{0eq}+3R_F}{(1-x)Z_{1L}+Z_{1G}+Z_{2eq}+Z_{0eq}+3R_F} \quad (13)$$

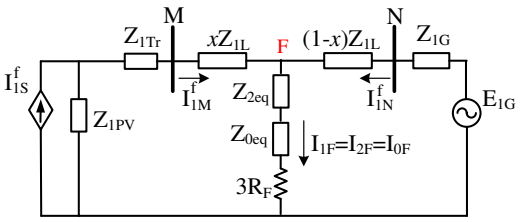

Fig. 7. Sequence network of solar plant integrated network for AG fault.

Considering negative sequence current to be negligible from the solar plant, phase-A currents at both ends of the line, for an internal AG fault, are expressed by,

$$\begin{aligned} I^f_{AM} &= I^f_{1M}+I^f_{0M} \\ I^f_{AN} &= I^f_{1N}+I^f_{2N}+I^f_{0N} \end{aligned} \quad (14)$$

Sequence networks being connected in series (as in Fig. 7), negative and zero sequence currents in the faulted path are influenced by I^f_{1M} and I^f_{1N}, and can be expressed as,

$$I_{1F}=I_{2F}=I_{0F}=I^f_{1M}+I^f_{1N} \quad (15)$$

From (12) and (15), sequence currents in the faulted path can be written as

$$I_{1F}=\frac{E_G}{(1-x)Z_{1L}+Z_{2eq}+Z_{0eq}+3R_F+Z_{1G}}+(1-k)I^f_{1S} \quad (16)$$

For a fault with very high R_F, the first part of (16) becomes very small and k close to 1 (as in (13)). These result in the faulted path current to be negligible. Thus the phase currents in (14) are mainly influenced by the positive sequence components. With very high R_F and k $\approx$ 1, the relation between I^f_{1M} and I^f_{1N} (in (12)) can be expressed by (17), which consequently represents the relation between phase-A currents at both ends for the situation.

$$I^f_{1M}=I^f_{1S}\approx -I^f_{1N} \quad (17)$$

Such similar magnitudes and phase opposition for phase currents at both ends of the line may result in maloperation of the differential relay. This is demonstrated in Fig. 8 with both percentage biased and α-plane characteristics for an AG fault with $R_F = 350\Omega$, created in line MN of the system in Fig. 1(a).

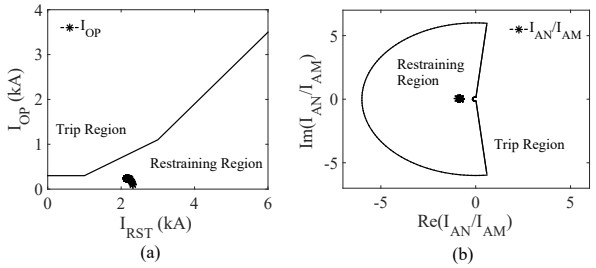

Fig. 8. Performance of differential relay for internal AG fault ($R_F = 350\Omega$) with (a) percentage biased and (b) α-plane characteristics.

As observed from the above cases, the current differential relays protecting lines connected to large scale solar plants may maloperate for faults with negligible R_F as well as with very high R_F. In both cases, negligible current in the faulted path results in relay maloperation. Thus there is a need for a new protection technique for proper discrimination of internal and external faults for such lines.

III. Proposed Method

Analysis in Section II reveals that the current differential relay protecting lines connected to large scale solar plants may malfunction in case of very severe faults (close to PV connected bus with $R_F \approx 0$) and also for faults with high R_F. For the former case, large phase angle separation between both end currents causes the faulted path current to be negligible in case of severe faults. For the latter case, high resistance in faulted path is the reason for the small faulted path current. To overcome such issues of differential relay during low faulted path current resulting due to two different reasons, a new protection method is proposed in this section by applying two criteria using both end incremental currents.

A. Criterion-1

For non-fault and external fault conditions, relation between phase-A currents at both ends can be expressed as,

$$I^{(pre,f)}_{AM}\approx -I^{(pre,f)}_{AN} \quad (18)$$

The relation between both end phase-A currents for an internal AG fault case can be expressed as,

$$I^f_{AM}+I^f_{AN}=I_{AF} \quad (19)$$

By subtracting the prefault components, the faulted path current in (19) can be expressed as the summation of both end incremental currents as in (20).

$$\Delta I_{AM}+\Delta I_{AN}=I_{AF} \quad (20)$$

where the incremental currents at both ends are expressed by,

$$\Delta I_{A(M,N)}=I^f_{A(M,N)}-I^{pre}_{A(M,N)} \quad (21)$$

Similarly, the summation of incremental currents becomes zero in the case of external faults. The summation may result in a spill current even for an external fault condition in case of CT saturation, which may only occur for faults between solar plant and bus M of Fig. 1 (a) for such connectivity due to the free flow of grid side currents at both ends. Note, this will not happen in case of external fault at the grid end due to the current from the solar plant being limited.

In order to analyze such a situation of external fault in the solar plant side, current measured at bus M is assumed to be $((K\angle\beta)I^f_{AM})$ instead of I^f_{AM} (K and β being magnitude and phase modulation due to saturation) and the other end not having saturation. The summation of both end incremental currents for such a situation can be expressed as,

$$\Delta I_{AM} + \Delta I_{AN} = (1 - K\angle\beta)I^f_{AN} \tag{22}$$

For a hard saturation condition, the maximum value of K and β are considered as 0.5 and 45^0 respectively [24]. With such a situation, the relation in (22) can be rewritten as,

$$|\Delta I_{AM} + \Delta I_{AN}| = 0.74|I^f_{AN}| \tag{23}$$

Further, using (19) and (20) the relation for internal faults can be expressed as

$$\Delta I_{AM} + \Delta I_{AN} = I^f_{AM} + I^f_{AN} \tag{24}$$

Comparing (23) and (24), the condition for internal fault detection can be written as,

$$|\Delta I_{AM} + \Delta I_{AN}| > 0.74|I^f_{AN}| \tag{25}$$

Dividing both sides by $|\Delta I_{AN}|$, (25) can be rewritten as in (26), which is considered as the criterion-1 for identifying internal faults using proposed method.

$$\left|\frac{\Delta I_{AM}}{\Delta I_{AN}} + 1\right| > 0.74\left|\frac{I^f_{AN}}{\Delta I_{AN}}\right| \tag{26}$$

Defining $\frac{\Delta I_{AM}}{\Delta I_{AN}} = a + jb$, (26) can be expressed as,

$$(a+1)^2 + b^2 > R^2 \tag{27}$$

where $R = 0.74\left|\frac{I^f_{AN}}{\Delta I_{AN}}\right|$.

The relation in (27) is represented by a circle (AZ_1) in complex plane, as shown in Fig. 9(a) with an adaptive radius R and the center located at (-1,0). $\frac{\Delta I_{AM}}{\Delta I_{AN}}$ is defined as index D_1 for identification of internal faults. Corresponding operating and restraining zones are shown in the figure.

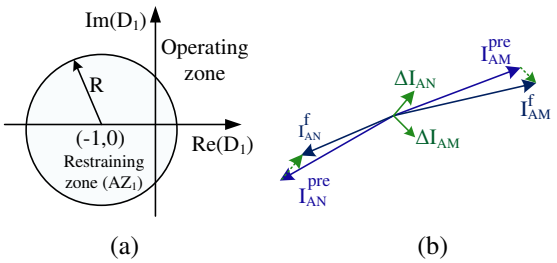

Fig. 9. (a) Adaptive operating characteristic for D_1 and (b) phasor diagram showing incremental currents for a high resistance fault situation.

It is observed that subtraction of prefault component in this approach makes the phase angle difference between both end incremental currents significantly lesser compared to the phase currents during fault, regardless of their resultant being equal (refer to (19) and (20)). Such a low phase angle difference provides high sensitivity in detecting internal faults in a low faulted path current situation. This is evident even for a high resistance fault condition (as mentioned in section II.B), shown in Fig. 9(b). The peculiarity of fault characteristics of a line connecting large scale solar plant prevents in exploring such an advantage while applied to a severe fault case close to PV connected bus. A large phase angle separation (close to 180^0) may be observed between the incremental currents along with the phase currents for such a situation. This is evident from the phasor diagram, shown in Fig. 10(a) for such a fault case (as mentioned in section II.A). In order to analyze such a situation, a pure-fault sequence network of a solar plant connected system of Fig. 4 for BC fault is introduced in Fig. 10(b), where Z^{pf}_{1SP} represents the pure-fault solar plant impedance including the transformer impedance [6].

For a severe fault close to PV connected bus, the index D_1 can be approximated to the ratio of positive sequence currents, as in (28), due to the presence of negligible negative and zero sequence currents in the faulted path (refer to section II.A).

$$D_1 = \frac{\Delta I_{AM}}{\Delta I_{AN}} \approx \frac{\Delta I_{1M}}{\Delta I_{1N}} \tag{28}$$

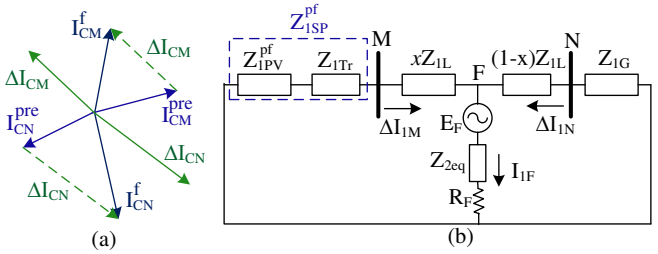

Fig. 10. (a) Phasor diagram for a severe BC fault close to bus M and (b) Pure-fault network of the system in Fig. 4 for a BC fault.

Applying current distribution property in Fig. 10(b), the ratio in (28) can be expressed as,

$$\frac{\Delta I_{1M}}{\Delta I_{1N}} = \frac{(1-x)Z_{1L} + Z_{1G}}{Z^{pf}_{1SP} + xZ_{1L}} \approx \frac{(1-x+K_1)Z_{1L}}{Z^{pf}_{1SP} + xZ_{1L}} \tag{29}$$

where Z_{1G} is expressed as a real valued multiplier (K_1) of Z_{1L}, considering the homogeneity in grid side transmission network [6]. For a fault close to bus M (i.e. $x \approx 0$), (29) can be rewritten as,

$$\frac{\Delta I_{1M}}{\Delta I_{1N}} \approx \frac{(1+K_1)Z_{1L}}{Z^{pf}_{1SP}} \tag{30}$$

From (30), the phase angle difference of both end currents can be expressed as,

$$\angle\Delta I_{1M} - \angle\Delta I_{1N} = \angle Z_{1L} - \angle Z^{pf}_{1SP} \tag{31}$$

Following NA-GC requirements Z^{pf}_{1SP} becomes more capacitive with increase in fault severity, which can be observed from a typical characteristic shown in Fig. 11(a) (obtained for the solar plant of Fig. 1(a)). This results in large phase angle separation between the incremental currents for severe faults close to bus M. On the other hand, the fault current limitation property of the solar plant raises the magnitude of Z^{pf}_{1SP} with the increase in fault severity, as observed in Fig. 11(b). This makes the magnitude ratio in (32) to be significant, which allows to adopt it as the second criterion in identifying internal

faults in such a situation for accurate relay decision, of course complementing the first one.

$$\left|\frac{\Delta I_{1N}}{\Delta I_{1M}}\right| = \frac{\left|Z_{1SP}^{pf}\right|}{|(1+K_1)Z_{1L}|} \tag{32}$$

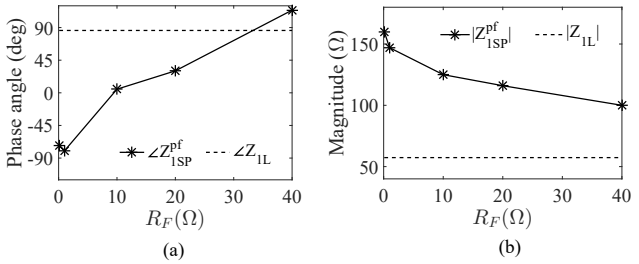

Fig. 11. Variation of a solar plant pure-fault impedance with fault resistances.

B. Criterion-2

As discussed above, a significant magnitude difference can be observed between both end positive sequence currents due to the fault current limit by the solar plant, especially in case of severe faults. For prefault and external fault conditions, the difference becomes negligible. Thus for detecting internal faults in such a situation, a condition as in (33) is included.

$$||\Delta I_{1N}| - |\Delta I_{1M}|| > \epsilon_1 \tag{33}$$

where the threshold ϵ_1 is set as in (34) considering maximum charging current difference between fault and prefault condition and associated measurement error [25].

$$\epsilon_1 = 1.1 I_{ch} \tag{34}$$

where, I_{ch} is the charging current in the line. Dividing both sides of (33) by $|\Delta I_{1M}|$, the relation can be rewritten as,

$$|D_2 - 1| > \frac{\epsilon_1}{|\Delta I_{1M}|} \tag{35}$$

where $D_2 = \frac{|\Delta I_{1N}|}{|\Delta I_{1M}|}$. (35) can be expanded as in (36), which is considered as criterion-2 for identifying internal faults.

$$D_2 < 1 - \frac{\epsilon_1}{|\Delta I_{1M}|} \quad or \quad D_2 > 1 + \frac{\epsilon_1}{|\Delta I_{1M}|} \tag{36}$$

The relation (36) represents a restraining region (AZ_2) with corresponding upper and lower limits adaptive to $|\Delta I_{1M}|$, as shown in Fig. 12.

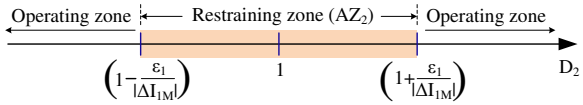

Fig. 12. Operating characteristic for index D_2.

External faults may mislead the decision obtained using D_2 in the presence of CT saturation. Negative sequence current from a solar plant (controlled in synchronous reference frame with feedforward compensation) is negligible, even for asymmetrical faults. Therefore a significant negative sequence current can only be observed at bus M for faults between the solar plant and bus M of Fig. 1(a). This is also the only fault situation possessing the chances of CT saturation. Thus comparison of negative sequence current at bus M (I_{2M}) with a threshold ϵ_2 can make the decision using D_2 secure. ϵ_2 is decided by the maximum negative sequence current present in the solar plant output during transient conditions and can be set as half of the rated current [26].

C. Logic Circuit for Proposed Adaptive Protection Method

Logic circuit for accomplishing the proposed adaptive protection technique is shown in Fig. 13. Following the current data acquisition from both ends, the proposed method calculates D_1 and D_2. Detection of D_1 outside AZ_1 confirms an internal fault situation. On the other hand, an internal fault can also be identified if I_{2M} is less than ϵ_2 and D_2 provides a value outside AZ_2 (defined by the limits as shown in Fig. 13). The proposed method issues a trip signal for the line end breakers following the detection of an internal fault situation by any of the indices, D_1 and D_2. The adaptivity in restraining zones for both the criteria maintains the balance between security and dependability for any system condition and their complementary nature makes the method suitable for lines connecting any type of sources irrespective of the associated control schemes.

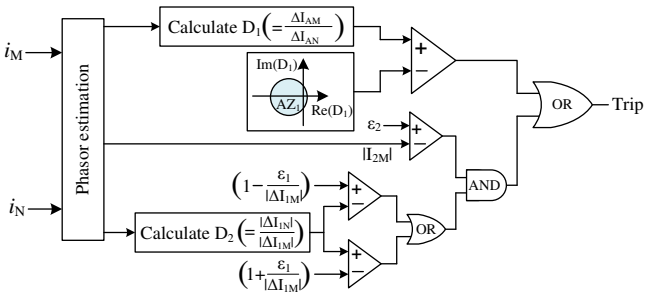

Fig. 13. Logic circuit for proposed protection technique.

IV. Results

The proposed method is tested for 345 kV, 60 Hz, 39-bus New England system [27] integrating solar plant, as shown in Fig. 14. Simulations are carried out using PSCAD/EMTDC. The synchronous generator connected at bus 29 is replaced by a 400 MW solar plant. Current data are obtained from both the ends of line 29-26 to evaluate the performance of the proposed adaptive protection technique for different fault conditions. Line 28-29 is disconnected from the system to emphasize the issue while current at one end of the faulted line is contributed only by the solar plant. In order to maintain the line flows similar to the standard system [27], loads at bus 28 and 29 are adjusted suitably. Current phasors are estimated using 1-cycle discrete Fourier transform with a sampling rate of 1.2 kHz. Comparative assessment with conventional approaches is provided to demonstrate the strength of the proposed method.

A. Performance of the proposed method for internal faults with different fault resistances and comparative assessment

Faults with different R_F values change the fault current modulation of the solar plant and affect the conventional differential relaying accordingly. In order to compare the performance of conventional differential approaches (percentage biased and α-plane) with the proposed method for faults with different R_F, phase-A-to-ground (AG) faults are created on line 26-29 at a distance of $0.1pu$ from bus 29. R_F is varied from 0.1Ω to 350Ω. Performance of the conventional current differential methods for such cases is shown in Fig. 15. Results

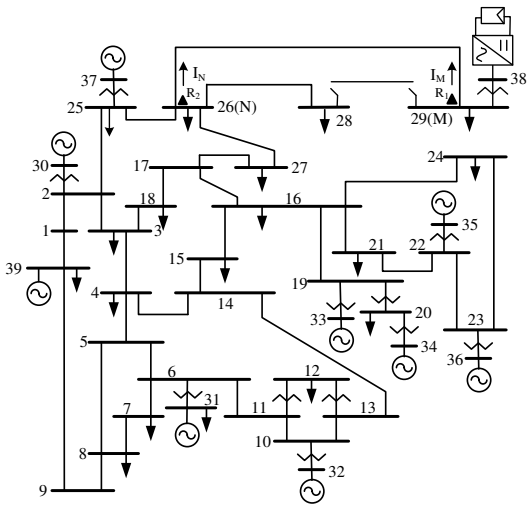

Fig. 14. New-England 39-bus integrated with PV plant.

demonstrate that the conventional approaches maloperate for faults with low R_F as well as with very high R_F. It is also observed that the α-plane based approach is more vulnerable for such situations compared to percentage biased approach. Indices D_1 and D_2 are calculated for all the cases and are shown in Fig. 16 with their corresponding adaptive restraining zones, AZ_1 and AZ_2 respectively. It is observed that D_1 values are outside the corresponding AZ_1 zones (satisfying criterion-1 for internal faults) except for faults with very low R_F (0.1Ω and 1Ω), where D_2 remains outside its AZ_2 zones (satisfying criterion-2). Faults being on line 26-29, negligible negative sequence currents are observed at solar plant connected bus (29) for all the cases. This ensures the correct identification of internal faults with different fault resistances by the proposed method and also shows its superiority compared to conventional approaches. Further, it is noticed that the two criteria supplement each other for reliable decisions.

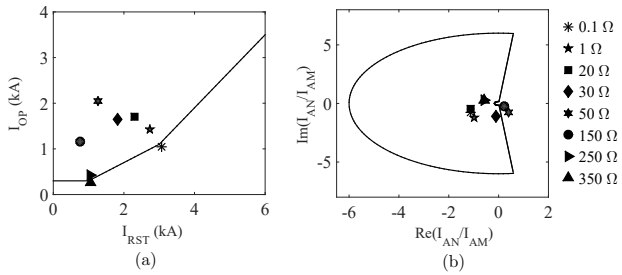

Fig. 15. Performance of (a) percentage biased and (b) α-plane based differential relay for AG faults with different fault resistances.

B. Performance of the proposed method for internal faults at different locations

Fault current contributions from both ends vary for internal faults at different locations on the line. This affects the performance of differential relaying. Phase-A-to-ground faults are created at different locations on line 29-26 with $R_F = 0.1\Omega$. Indices D_1 and D_2 are calculated for all the fault cases and are shown in Fig. 17 with their corresponding adaptive restraining zones. It is observed that the calculated D_1 values are inside the corresponding restraining zones (AZ_1) for all the cases except the internal fault at $0.95pu$ from bus 29. Thus the proposed method fails to satisfy criterion-1 for such internal fault situations. On the other hand, D_2 values, calculated for all the cases remain outside the corresponding AZ_2 zones (satisfying criterion-2) with negligible I_{2M} and confirms the detection of all the internal faults correctly complementing criterion-1.

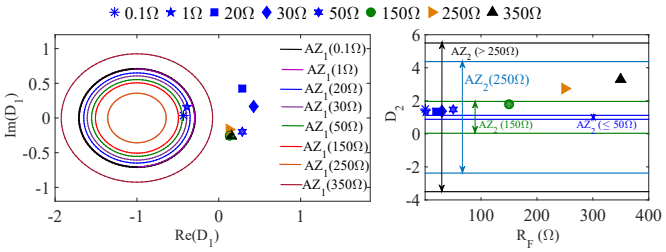

Fig. 16. Performance of the proposed method for faults with different R_F.

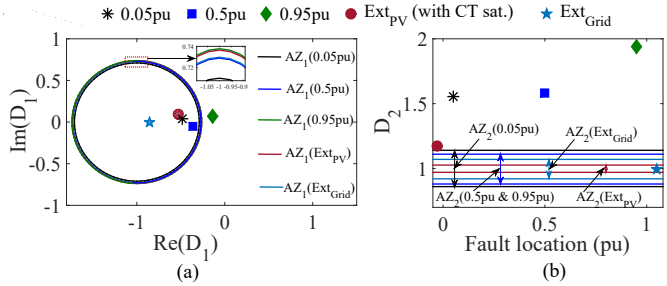

Fig. 17. D_1 and D_2 calculated for faults created at different locations.

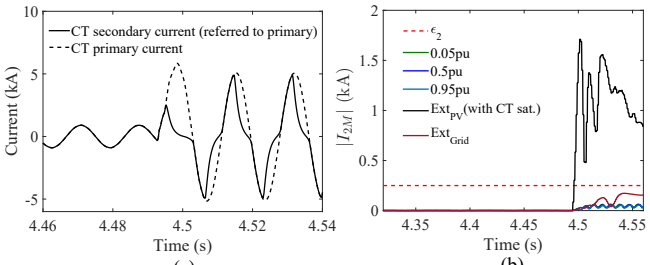

Fig. 18. (a) CT currents for the saturation case and (b) security provided by negative sequence current in case of CT saturation.

C. Performance of the proposed method for external faults

External faults with CT saturation may maloperate the conventional differential relay. In order to evaluate the performance of the proposed method in such situations, bolted 3-phase external faults are created at PV and grid sides close to the respective line ends. External fault close to PV connected bus (29) results in CT saturation at bus 29. Indices D_1 and D_2 calculated for both the cases are shown in Fig. 17 with their corresponding adaptive restraining zones. Primary fault current (phase-A) and corresponding CT secondary current (referred to primary) for the saturation case are shown in Fig. 18(a). Fig. 18(b) shows that I_{2M} is higher than the threshold (ϵ_2) only for the PV side external fault case. It is observed that D_1 for both the cases are outside corresponding AZ_1 zones and satisfies criterion-1 for external fault conditions. On the other hand, D_2 satisfies criterion-2 only for grid side external fault, whereas falsely detect the PV side external fault as an internal fault due to CT saturation. Significant I_{2M} observed

at bus 29 for such a situation prevents the tripping operation. This shows the reliability in using the proposed technique for external faults with and without CT saturation.

D. Performance of the proposed method for internal faults with different solar plant generations

Fault current contribution from a solar plant changes with its generation, which varies with the number of available operating units in the plant. Reduction in solar plant generation makes the magnitude difference of both end fault currents to be prominent and reduces the chances of differential relay maloperation, as observed earlier for lines connecting a large scale solar plant. This is evident from the results shown in Fig. 19, for phase-B-to-phase-C (BC) faults at a distance of 0.05 pu from bus 29 with $R_F = 0.1\ \Omega$. The solar plant generation is varied from 100 MW to 400 MW by changing the number of operating units in the plant and the maloperation is observed in phase-C for the cases. Results show that conventional differential relay with both the approaches fails to identify the internal faults with solar plant generation of 300 MW and 400 MW, whereas the detection will be correct when the plant generation reduces to 100 MW. Fig. 20 demonstrates the performance of the proposed method with D_1 and D_2 for all the cases with different solar plant generations. Faults being on line 26-29, negligible I_{2M} is observed at bus 29 for all the cases. It is found that the proposed method identifies the internal faults correctly for all the cases. As the faults are created close to the solar plant connected bus with low R_F, the decision using D_2 (satisfying criterion-2) is found to be more promising in the decision process with the proposed method. This demonstrates the superiority of the proposed method compared to conventional approaches even with variation in solar plant output.

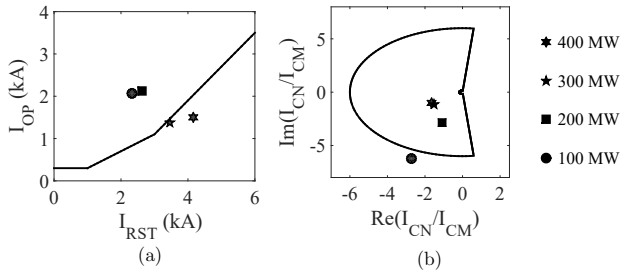

Fig. 19. Performance of (a) percentage biased and (b) α-plane based differential relay for BC faults with different solar plant generations.

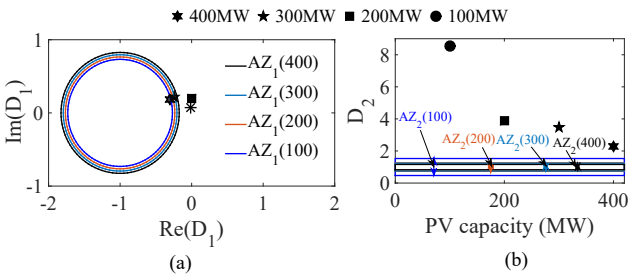

Fig. 20. D_1 and D_2 calculated for faults with different solar plant capacities.

E. Performance of the Proposed Method for different line lengths

Fault current from the grid reduces with an increase in the length of the connecting line. This influences the operation of current differential relay for the line connecting solar plants and may result in erroneous operation at times, which is already analyzed in Section II. Performance of the proposed method is tested now for such a condition, where the length of the connecting line (line 29-26) is considered as 20 km, 160 km, and 200 km at a time. Fig. 21 demonstrates the performance of the proposed method for AG faults (with $R_F = 0.1\Omega$) created at a distance of $0.1pu$ from bus 29, with D_1 and D_2 calculated for all the cases. It is observed that for fault in a short line (with L = 20km), both the indices detect the fault correctly, whereas for long lines one of the indices only detects the fault correctly. As severe faults are created near the solar plant connected bus, D_2 ensures the correct fault detection for all the cases.

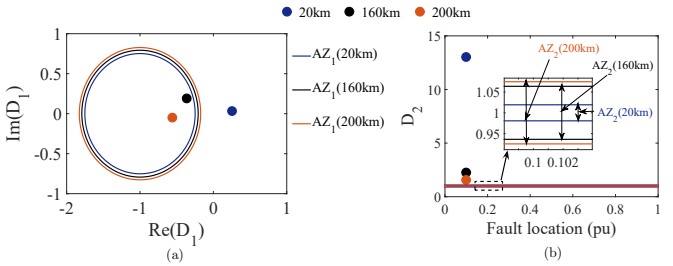

Fig. 21. D_1 and D_2 calculated for internal faults in a solar plant connecting line with different lengths.

F. Performance of the proposed Method in the presence of measurement noises

1-cycle DFT and the antialiasing low-pass filter can mitigate the effect of noise in the proposed method. In order to evaluate the performance of the proposed method under noisy conditions, current signals are contaminated with uniform distribution noise with zero mean and a standard deviation of 2% [28] for an AG fault created in line 29-26 at a distance of $0.1pu$ from bus 29 with $R_F = 0.1\Omega$. D_1 and D_2 calculated by the proposed method for such a situation are shown in Fig. 22. Results demonstrate the effectiveness of the proposed method even in the presence of measurement noises.

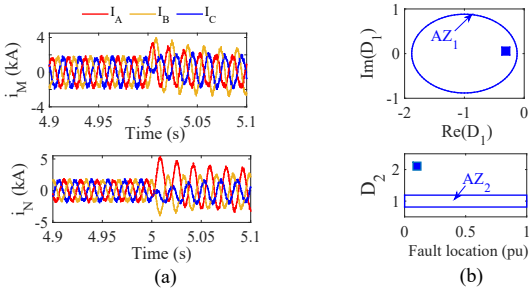

Fig. 22. (a) Currents with noise contaminant and (b) D_1 and D_2 calculated for an internal fault in the presence of measurement noises.

G. Performance of the proposed method in the presence of harmonics

In order to test the performance of the proposed unit protection technique in the presence of harmonics, the current signals measured at the solar plant connected bus are contaminated with all the lower order harmonics ($\leq 5^{th}$ order), as per IEEE Std. 519-1992. Higher order harmonics are filtered out using the anti-aliasing filter. An AC fault is created at a distance of $0.1pu$ from bus 29 with $R_F = 0.1\Omega$. Results in Fig. 23 demonstrate the correct performance of the proposed method with harmonic contaminated current signals.

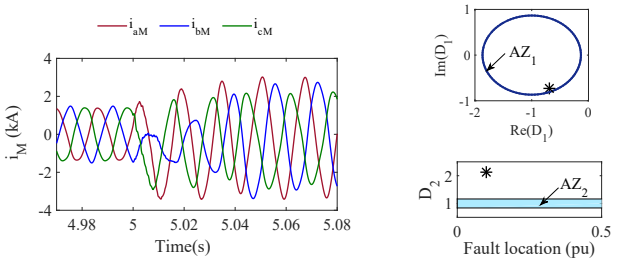

Fig. 23. (a) Harmonic contaminated current signal and (b) D_1 and D_2 calculated for an internal fault in the presence of current harmonics.

H. Performance of the proposed method for fault during unbalance condition

Proposed method using incremental phase and positive sequence currents remain unaffected by the unbalance situation in power systems. Performance of the proposed method is tested for such a condition. An AG fault is created in line 29-26. The fault is cleared by opening the both end circuit breakers of phase-A. In such an unbalanced condition a BG fault is created on the same line at a distance of $0.1pu$ from bus 29 with $\mathrm{R_F} = 0.1\Omega$. Both end currents observed for such a situation are shown in Fig. 24. Results in Fig. 25 demonstrate that D_1 and D_2 calculated by the proposed method satisfy both the criteria for fault detection and the method performs correctly in such a situation.

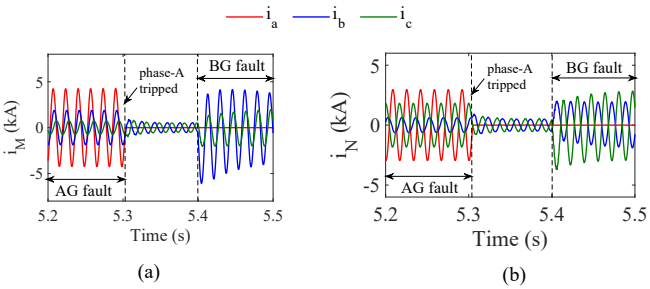

Fig. 24. Currents observed at (a) bus 29 (M) and (a) bus 26 (N) for fault in an unbalanced condition.

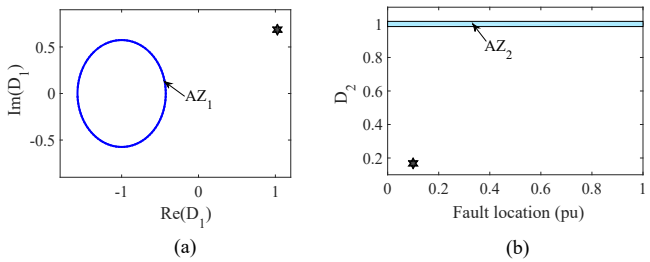

Fig. 25. D_1 and D_2 calculated for an internal fault during unbalanced condition.

I. Performance of the proposed method with different renewable power plants complying different grid code

Fault current characteristic of renewable plant changes with grid code requirements and also with associated control schemes. In order to evaluate the performance of the proposed method for both conditions, two separate case studies are performed. In the first case, the European grid code (EU-GC) is applied to the solar plant, which enables the plant to provide sufficient reactive power support compared to NA-GC. Results provided in Fig. 26 shows the active and reactive current generated for the situation and also demonstrates the performance of the proposed method for an AG fault, created in line 29-26 at a distance of $0.1\ pu$ from bus 29 with $R_F = 0.1\Omega$. In the second case, the solar plant of Fig. 1(a) is replaced by a Type-III and a Type-IV wind farm, one at a time. D_1 and D_2 calculated for similar fault situations are provided in Fig. 27. Results demonstrate that the proposed method using D_1 and D_2 can identify the faults correctly for all the cases. This shows the applicability of the method for different renewable sources with changes in grid code as well as associated control schemes.

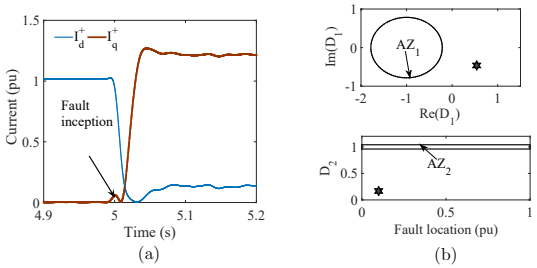

Fig. 26. (a) Active and reactive current generation and (b) D_1 and D_2 calculated for faults in a line connecting solar plant with EU-GC compliance.

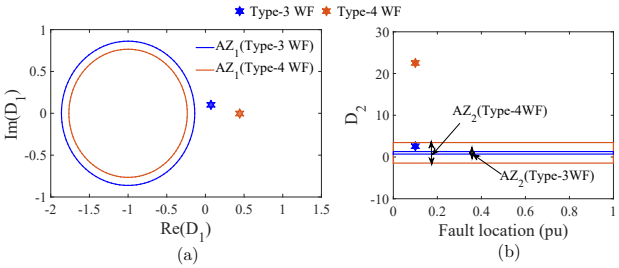

Fig. 27. D_1 and D_2 calculated for faults with different wind farms.

J. Performance of the Proposed Method for different test systems

The performance of the proposed method is now tested for other two standard systems integrating solar plants. The first one is a WSCC 9-bus system integrating a 400 MW solar plant at bus 9, as in [17]. The second one is an IEEE 118-bus system [29], where a 400 MW solar plant is connected at bus 112. The proposed method is tested for faults in the solar plant connecting line, maintaining the line length same for all the cases. An AG fault is created at a distance of $0.1\ pu$ from the solar plant connected bus with $R_F = 1\Omega$. Large interconnections make the grid strong and reduce the chance of differential relay maloperation. This is observed from the results shown in Fig. 28. Both the conventional approaches perform correctly for the IEEE 118-bus system, whereas fail for the WSCC 9-bus system. Fig. 29 demonstrate the correct performance of the proposed method for different power systems.

K. Comparative Assessment with available methods

A comparative assessment of the proposed method with recently available techniques is summarized in Table I. The composite sequence current based approach of [13], current similarity based approach of [12] and magnitude ratio based

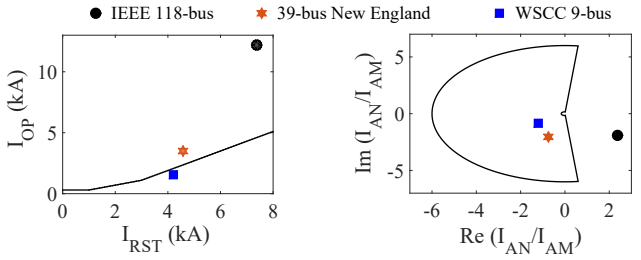

Fig. 28. Performance of conventional differential relay for different test systems with (a) percentage biased and (b) α-plane based characteristics.

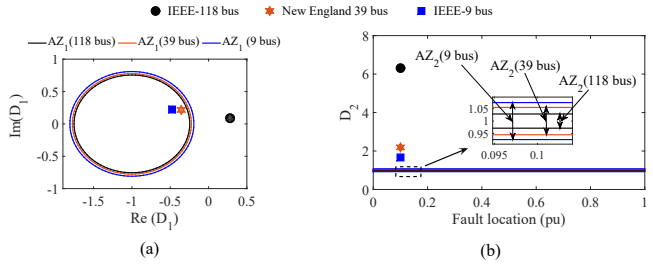

Fig. 29. Performance of proposed method for different test systems.

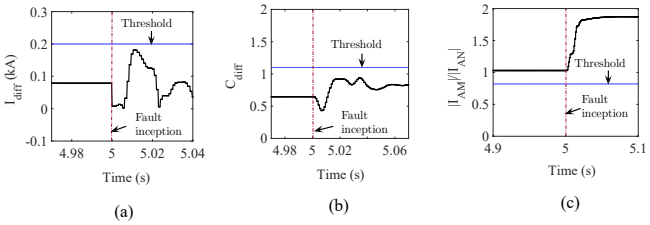

Fig. 30. Performance of available differential methods in [13] and [14] for two fault conditions.

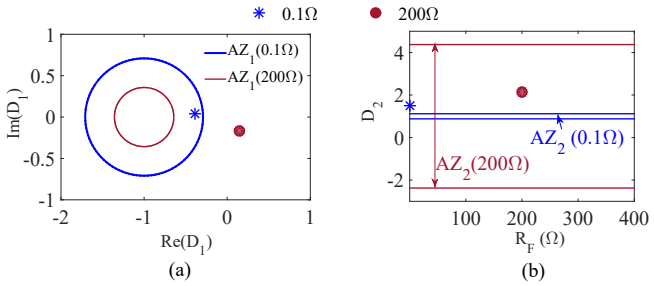

Fig. 31. Performance of the proposed method for two different faults.

approach of [14] are considered for this assessment. The table clearly depicts that the incremental current ratio based proposed method is superior compared to the recently available methods for protecting a solar plant connected line. In addition to that the performance of the methods available in [13] and [14] are tested for a 3-phase fault with $R_F = 0.1\Omega$ and an AG fault with $R_F = 200\Omega$ respectively. Both the faults are created in line 29-26 at a distance of 0.05 pu from bus 29. I_{diff} and C_{diff} in Fig. 30(a) and Fig. 30(b) below the corresponding threshold indicates the maloperation of the method in [13] for the 3-phase fault situation. On the other hand, the magnitude ratio in Fig. 30(c) is above the corresponding threshold, which also indicates the maloperation of the method in [14]. Results in Fig. 31 demonstrate the correct performance of the proposed method for both the cases, which show its strength over those methods.

TABLE I
COMPARATIVE ASSESSMENT WITH AVAILABLE METHODS

Parameters	Available Methods			Proposed Method
	[9]	[11]	[12]	
Sensitive to all types of faults?	No	Yes	Yes	Yes
Performance for high resistance fault	Satisfactory	Satisfactory	Not satisfactory	Satisfactory
Affected by noise?	No	Yes	No	No
Applicable to weak grid condition?	No	Yes	No	Yes
Affected by CT saturation?	Yes	Yes	Yes	No
Ability to operate in single infeed condition?	Yes	No	Yes	Yes

V. REAL-TIME VALIDATION

The proposed method is validated using OP4510 (OPAL-RT) real-time simulator. Fig. 32 shows the real-time simulation experimental setup used for this work. Parameters associated with real-time simulator are provided in Table II. The renewable integrated 39-bus New England system and the proposed unit protection method are modeled in MATLAB integrated with OPAL-RT, which are compiled with RT-LAB to run as an effective platform for developing and testing the real-time operation of the proposed method.

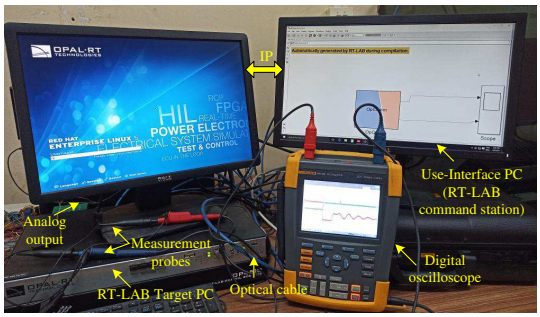

Fig. 32. Real-time simulation (OPAL-RT) experimental setup.

A 3-phase fault with $R_F = 0.1\Omega$ and an AG fault with $R_F = 200\Omega$ are created in line 29-26 at a distance of 0.1 pu from bus 29. Conditions in (26) and (35) are checked to test the performance of the proposed method using both criteria. Results obtained for both the situations are provided in Fig. 33, which demonstrate that the proposed method can correctly detect the 3-phase severe fault using criterion-2, whereas criterion-1 is found to be promising in case of high resistance AG fault. This validates the real-time performance of the proposed method.

TABLE II
PARAMETERS ASSOCIATED WITH OPAL-RT SIMULATOR

Parameters	Description
Time step	100 μs
Operating system	Linux based Redhat OS
Simulator	OP4510 (RCP/ HIL vitex7 FPGA processor)

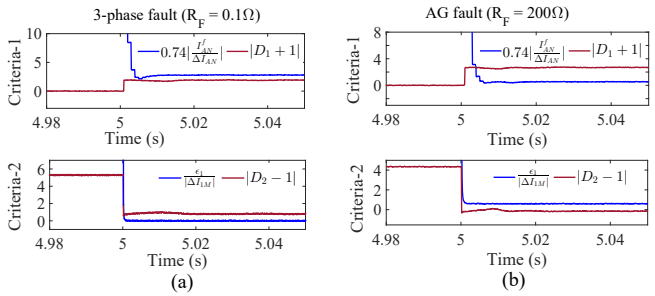

Fig. 33. Real-time performance of the proposed method for (a) a 3-phase fault with $R_F = 0.1\Omega$ and (b) an AG fault with $R_F = 200\Omega$.

VI. Conclusion

The fault current signature contributed by solar plants is different because of numerous control schemes embedded in it. Line differential protection finds limitations, in particular for the situation when grid side contribution becomes comparable to solar plant during fault. A method comprising two indices, representing the ratio of incremental phase currents and the magnitude ratio of both end positive sequence incremental currents are proposed for the identification of internal faults with such connectivity. The restraining zones corresponding to the indices are adaptive to line end currents and provide high dependability for internal fault detection. An additional check of negative sequence current at the solar plant connected bus enhances the security of the proposed method during CT saturation. Results demonstrate the accurate performance of the proposed method for variation in fault resistance, fault location, and solar plant output. The applicability of the proposed method is also demonstrated for lines connecting different renewable sources with different grid code compliances. Accurate performance for challenging situations like unbalanced conditions, presence of measurement noises and harmonics demonstrate the robustness of the proposed method. The compatibility of the proposed approach is checked with a real-time simulator. Comparative assessment with conventional techniques reveals its superiority.

Appendix

TABLE III
Simulation Parameters of the System in Fig. 1

Element	Parameter	Value
PV plant	Unit capacity	1 MW
	Total number of units	400
Transformer	Voltage level, Frequency	33/230 kV, 60Hz,
	Vector group	YNd11
	MVA, %Z	500 MVA, 7%
Transmission line	Voltage, Line length	230 kV, 200 km
	Positive sequence impedance	0.02+j0.28 Ω/km
	Zero sequence impedance	0.106+j0.84 Ω/km
	Positive sequence susceptance	273.55 MΩ-m
	Zero sequence susceptance	414.16 MΩ-m
PI controller	Current controller (d-q axis)	K_P = 0.15 T_i = 0.08 s
DC bus	Rated voltage	600 V
	DC link capacitor	7800 μF
Filter	L_f. C_f, R_f	300μH, 200μF, 0.025Ω

References

[1] "648 MW, Kamuthi, Tamil Nadu," Adani renewables, [Online]. Available: https://www.adanigreenenergy.com/solar-power/Kamuthi.

[2] "Green Energy Corridors II (Part-A): A Plan for Integration of Ultra Mega Solar Power Parks," Power Grid Corporation of India Ltd. [Online]. Available: https://www.powergridindia.com/sites/default/files/Our_Business/Smart-_Grid/2017/1/Green%20Energy%20Corridor%202-Part%20A.pdf.

[3] Y. Wang and B. Ren, "Fault ride-through enhancement for grid-tied PV systems with robust control," *IEEE Trans. Ind. Electr.*, vol. 65, no. 3, pp. 2302–2312, March 2018.

[4] K. Jia, Z. Yang, Y. Fang, T. Bi, and M. Sumner, "Influence of inverter-interfaced renewable energy generators on directional relay and an improved scheme," *IEEE Trans. Power Electr.*, vol. 34, no. 12, pp. 11 843–11 855, Dec 2019.

[5] A. Hooshyar, M. A. Azzouz, and E. F. El-Saadany, "Distance protection of lines emanating from full-scale converter-interfaced renewable energy power plants Part-I: Problem statement," *IEEE Trans. Power Del.*, vol. 30, no. 4, pp. 1770–1780, Aug 2015.

[6] S. Paladhi and A. K. Pradhan, "Adaptive distance protection for lines connecting converter-interfaced renewable plants," *IEEE J. Emerg. Sel. Topics Power Electron.*, available in early access.

[7] S. Paladhi and A. K. Pradhan, "Adaptive fault type classification for transmission network connecting converter-interfaced renewable plants," *IEEE Syst. J.*, available in early access.

[8] Y. Xue, B. Kasztenny, D. Taylor, and Y. Xia, "Series compensation, power swings, and inverter-based sources and their impact on line current differential protection," in *Proc. 66th Annual Conf. Prot. Relay Engineers*, April 2013, pp. 80–91.

[9] B. Mackie, and C. Palmer, "Summary paper for C37.243 IEEE Guide for application of digital line current differential relays using digital communication," in *70th Annual Conference for Protective Relay Engineers (CPRE)*, 2017, pp. 1–8.

[10] "Modern techniques for protecting and monitoring of transmission lines," CIGRE working group B.5.07, June 2011.

[11] Y. Li, K. Jia, T. Bi, R. Yan, W. Li, and B. Liu, "Analysis of line current differential protection considering inverter-interfaced renewable energy power plants," in *Proc. IEEE PES Innov. Smart Grid Techn. Conf. Europe*, Sep. 2017, pp. 1–6.

[12] K. Jia, Y. Li, Y. Fang, L. Zheng, T. Bi, and Q. Yang, "Transient current similarity based protection for wind farm transmission lines," *Applied energy*, vol. 225, pp. 42–51, 2018.

[13] S. Chen, N. Tai, C. Fan, J. Liu, and S. Hong, "Sequence-component-based current differential protection for transmission lines connected with IIGs," *IET Gen., Trans. Distr.*, vol. 12, no. 12, pp. 3086–3096, 2018.

[14] K. Jia, Z. Yang, Z. Zhu, Y. Fang, Q. Zhao, and B. Liu, "Current amplitude ratio based pilot protection for the transmission line connected to inverter-interfaced renewable energy power plants," in *Proc. IEEE Innov. Smart Grid Techn. - Asia*, May 2019, pp. 2090–2094.

[15] H. J. A. Ferrer (editor) and E. O. Schweitzer III (editor), *Modern solutions for protection, control, and monitoring of electric power systems*. Pullman, WA, Schweitzer Eng. Lab., 2010, pp. 84–89.

[16] A. Yazdani and R. Iravani, *Voltage-Sourced Converters in Power Systems: Modeling, Control, and Applications*. Hoboken, NJ, USA: Wiley, 2010.

[17] A. Banaiemoqadam, A. Hooshyar, and M. A. Azzouz, "A control-based solution for distance protection of lines connected to converter-interfaced sources during asymmetrical faults," *IEEE Trans. Power Del.*, vol. 35, no. 3, pp. 1455-1466, June 2020.

[18] "Reliability guideline: BPS-connected inverter-based resource performance," North American Electric Reliability Corporation, Atlanta, GA, Tech. Rep., September 2018.

[19] Y. Bae, T. Vu, and R. Kim, "Implemental control strategy for grid stabilization of grid-connected PV system based on German grid code in symmetrical low-to-medium voltage Network," *IEEE Trans. Energy Conv.*, vol. 28, no. 3, pp. 619-631, Sept. 2013.

[20] J. Rocabert, A. Luna, F. Blaabjerg, and P. Rodrguez, "Control of power converters in AC microgrids," *IEEE Trans. Power Electr.*, vol. 27, no. 11, pp. 4734–4749, 2012.

[21] "Line differential protection RED670," June 2010, application manual.

[22] "SEL-311l-1, -7 relay protection and automation system," 2011, instruction manual.

[23] Z. Y. Xu, Z. Q. Du, L. Ran, Y. K. Wu, Q. X. Yang, and J. L. He, "A current differential relay for a 1000-kV UHV transmission line," *IEEE Trans. Power Del.*, vol. 22, no. 3, pp. 1392–1399, 2007.

[24] B. Kasztenny, G. Benmouyal, H. J. Altuve, and N. Fischer, "Tutorial on operating characteristics of microprocessor-based multiterminal line current differential relays," *Sci. papers of the Inst. of Electr. Power Eng. of the Wroclaw University of Tech.*, 2013.
[25] J. Bell, A. Hargrave, G. Smelich, and B. Smyth, "Considerations when using charging current compensation in line current differential applications," in *Proc. 72nd Annual Conf. Protective Relay Engineers*, March 2019, pp. 1–11.
[26] G. Kou, L. Chen, P. VanSant, F. Velez-Cedeno, and Y. Liu, "Fault characteristics of distributed solar generation," *IEEE Trans. Power Del.*, vol. 35, no. 2, pp. 1062–1064, 2020.
[27] I. Hiskens, "IEEE PES task force on benchmark systems for stability controls," Tech. Rep., November 2013.
[28] J. G. Rao, and A. K. Pradhan, "Power-swing detection using moving window averaging of current signals," *IEEE Trans. Power Del.*, vol. 30, no. 1, pp. 368-376, Feb. 2015.
[29] S. Paladhi, and A. K. Pradhan, "Resilient protection scheme preserving system integrity during stressed condition," *IET Gen., Trans. Distr.*, vol. 13, no. 14, pp. 3188–3194, 2019.

Arghadeep Chowdhury is currently working toward the Ph.D. degree in the Department of Electrical Engineering at the Indian Institute of Technology, Kharagpur, India.

Subhadeep Paladhi is currently working toward the Ph.D. degree in the Department of Electrical Engineering at the Indian Institute of Technology, Kharagpur, India.

Ashok Kumar Pradhan is a Professor in the Department of Electrical Engineering, Indian Institute of Technology, Kharagpur, India.